

1 A mineralogical signature for Burgess Shale-type 2 fossilization

3 **Ross P. Anderson^{1,2,3*}, Nicholas J. Tosca³, Robert R. Gaines⁴, Nicolás Mongiardino**
4 **Koch¹, and Derek E.G. Briggs^{1,5}**

5 *¹Department of Geology and Geophysics, Yale University, New Haven, Connecticut*
6 *06511, USA*

7 *²All Souls College, University of Oxford, Oxford OX1 4AL, UK*

8 *³Department of Earth Sciences, University of Oxford, Oxford OX1 3AN, UK*

9 *⁴Geology Department, Pomona College, Claremont, California 91711, USA*

10 *⁵Peabody Museum of Natural History, Yale University, New Haven, Connecticut 06520,*
11 *USA*

12 *E-mail: ross.anderson@all-souls.ox.ac.uk

13 **ABSTRACT**

14 Burgess Shale-type (BST) fossilization of carbonaceous remains that are
15 ordinarily lost to decay is critical to our understanding of the early evolution of complex
16 life. Sediment composition, particularly the abundance of certain clay minerals, has been
17 invoked as a significant factor in BST fossilization. X-ray diffraction data for 213
18 Cambrian shales from 19 sedimentary successions on four continents provide the first
19 comprehensive test of the association of clay mineral assemblages with BST fossils.
20 Samples containing BST fossils yield mineralogical compositions that form a subset
21 within the range represented by samples containing only fossil mineralized skeletons.
22 Logistic regression and classification tree methods reveal that BST fossils are more likely

to be found in sediments rich in berthierine/chamosite and poor in celadonite and illite.

This characteristic clay mineralogy probably reflects a high kaolinite/smectite ratio in the original sediment and enhanced iron availability during early diagenesis. Models derived from both methods can predict the occurrence of BST fossils in fossiliferous samples based on clay mineralogy with ~80% accuracy, providing a mineralogical signature that may be useful in refining the search for BST fossils on Earth and beyond.

INTRODUCTION

Burgess Shale-type (BST) fossilization, which preserves decay-prone organic remains as carbonaceous compressions in fully marine fine-grained siliciclastic sediments (see Butterfield, 1995 for definition), has been crucial to our understanding of the Cambrian Explosion—one of the most significant events in the history of life. Wholly non-mineralized organisms account for ~86% of generic richness (Conway Morris, 1986; see also Caron and Jackson, 2006) in the Phyllopod Bed of the famed Burgess Shale; without them we would have a very incomplete picture of animal life in Cambrian seas. BST fossils are not just a macroscopic phenomenon but reveal a microscopic Cambrian diversity—in small carbonaceous fossils (SCFs) (e.g., Butterfield and Harvey, 2012). BST fossilization may be even more important to our understanding of Proterozoic eukaryotic evolution, before the advent of widespread biomineralization: a recent compilation of early eukaryotes shows that 47 of 59 localities yielding organic-walled microfossils preserve them in fine-grained siliciclastics (some including forms more fragile/decay-prone than the typical recalcitrant spheroidal acritarchs/palynomorphs) (Cohen and Macdonald, 2015).

Over the last three decades there has been a substantial effort to understand the preservation of these exceptional fossils, because it is vital to interpretations of their ecology (e.g., Gaines, 2014). One of the factors proposed as being important to BST fossilization is sediment composition, in particular clay mineralogy. The siliciclastic sediments that preserve BST fossils have high clay-to-organic ratios, and clay minerals have been posited to facilitate exceptional preservation by binding to autolytic enzymes, rendering them inactive and slowing the rate of decay (Butterfield, 1990, 1995). The effect of clay mineralogy has received renewed attention in recent experimental studies. Carcasses of polychaetes and crustaceans were preserved with higher fidelity when decayed in the presence of the aluminum-rich clay mineral kaolinite (this was attributed to the effect of this mineral in polymerizing tissue components in a process analogous to tanning, increasing their resistance to decay: Wilson and Butterfield, 2014; Naimark et al., 2016a; Naimark et al., 2016b). In an additional study, the growth of a heterotrophic bacterium, involved in the decay of marine organisms today, was shown to be inhibited in the presence of both kaolinite and berthierine (an iron-rich clay mineral) (McMahon et al., 2016).

Although this recent experimental evidence supports the hypothesis that clay minerals may be important in promoting BST fossilization, few studies have attempted to relate the distribution of BST fossils to that of sedimentary strata with a particular clay mineral composition. Previous research found limited evidence of particular associations, focusing only on a few individual fossiliferous formations (e.g., Aitken et al., 1973; Odom, 1976; Rolf et al., 1977; Butterfield, 1994; Powell, 2003; Curtin and Gaines, 2011; Gaines et al., 2011; Forchielli et al., 2014; Gaines, 2014). Here we explore the

relationship between BST fossils (focusing only on macroscopic Cambrian BST fossils) and particular suites of clay minerals.

MATERIALS AND METHODS

The mineralogy of Cambrian shale samples that contain BST fossils ($n = 131$) was compared with those that yield only fossil mineralized skeletons ($n = 82$). Samples were derived from 19 sedimentary successions distributed on four continents (mean samples per succession = 10.7, range = 1–58, see GSA Data Repository for description of sample selection protocol). Only the relationship between clay mineralogy and macroscopic Cambrian BST fossils was investigated, as it is difficult to obtain a large sample suite of lithologies that have been processed and yield or do not yield delicate microscopic fossils such as Cambrian SCFs or Proterozoic organic-walled microfossils. Matrix materials from each sample were prepared as randomly orientated powdered aggregates (ground to $\sim 10\mu\text{m}$) on single crystal silicon substrates 27 mm in diameter, and X-ray diffraction (XRD) was performed using a PANalytical Empyrean diffractometer, employing a Co $K\alpha$ source and PIXcel-1D detector.

Semiquantitative bulk mineralogy, including the total fraction of the sample comprising clay minerals, was obtained from diffraction patterns over the range $5\text{--}80^\circ 2\theta$, which were analyzed using the ICDD Powder Diffraction File-4+ database and the reference intensity ratio method (Snyder and Bish, 1989). However, to differentiate and quantify individual clay mineral species, XRD data were collected from the region $69\text{--}75^\circ 2\theta$, which yields weak but diagnostic peaks for different clay minerals commonly manifested as a composite reflection arising from 060 and/or 33–1 (Środoń et al., 2001). The areas of these peaks are a linear function of the relative abundance of different clays

as a proportion of the total clay fraction (Środoń et al., 2001). Berthierine/chamosite, glauconite, celadonite, illite of two distinct compositions (differentiated by consistently offset 060 reflections, with composition 1 likely containing a higher proportion of iron), and kaolinite were the principal clay minerals identified (see GSA Data Repository Figure 1 for frequency distributions of 060 reflections). For simplicity, berthierine and chamosite were grouped; the latter is an Fe-rich chlorite commonly derived from the burial metamorphism of berthierine (Hornibrook and Longstaffe, 1996). An estimate of the proportion of the rock composed of each clay mineral was obtained by multiplying the relative abundance calculated from the 060 region by the total clay fraction obtained from the bulk analysis; we term the resulting value “clay abundance”. This estimate incorporates some uncertainty resulting from the determination of the *total clay* fraction based on the bulk analysis (see GSA Data Repository). However, this uncertainty does not affect relative clay mineral abundances determined from 060 reflections.

Statistical analyses were executed using the R programming language (R Development Core Team, 2016) in order to determine the nature of the relationship between the type of preservation and the abundances of clay minerals (for detailed methodology see GSA Data Repository). The statistical methods used make no assumptions regarding the underlying distribution of the variables, and are robust to different types of relationships between response and predictors, as well as to the presence of interactions among the latter. Sensitivity tests were performed and are discussed in the GSA Data Repository.

RESULTS

Condensing variability in clay mineral abundance into two-dimensional space (Fig. 1) on principal coordinate axes (PCoA) shows that samples that contain BST fossils occupy a subset of the space occupied by those that contain only fossil mineralized skeletons. The position of the two groups is significantly offset (PERMANOVA, $R^2 = 0.14$, $F = 33.1$, $P < 10^{-5}$), indicating systematic differences in clay mineral composition between them. The variance of both groups also differs significantly (PERMDISP, $F = 176$, $P < 10^{-5}$): samples bearing BST fossils display a variance in clay assemblages only 36% of that of samples with only fossil mineralized skeletons. The frequency distributions in Figure 1 confirm that samples containing BST fossils occupy a portion of space that is both more restricted and centered around a different region to that occupied by the other samples. 70% of samples containing BST fossils cluster in a small region between -15 and 0 PCoA1, and -15 and 5 PCoA2, where only 12% of samples with fossil mineralized skeletons are found. The limited dispersion shown by samples containing BST fossils is not a product of reduced sampling, as BST fossil-bearing samples constitute ~62% of the total number.

A best fit multiple logistic regression model (Fig. 2) reveals that the abundance of illite composition 1, illite composition 2, berthierine/chamosite, and celadonite has a significant effect on the chances that a sample will contain BST fossils (Likelihood Ratio Test for sequential variable incorporation, $P = 1.8e^{-12}$, $9.5e^{-6}$, $3.7e^{-5}$ and $4.0e^{-3}$, respectively; the abundances of either glauconite or kaolinite had no significant effect). Samples with >50% of illite composition 1 have negligible probabilities of containing BST fossils, and those with >50% of illite composition 2 have probabilities below 0.3. Increasing the abundance of celadonite has a similar but less pronounced effect. In

contrast, higher abundance of berthierine/chamosite increases the probability that a sample will contain BST fossils, a probability that exceeds 0.9 for samples with greater than 20% berthierine/chamosite.

A conditional inference classification tree (Fig. 3) shows a strong concordance with the results of the multiple logistic regression. The abundance of illite composition 1 has the strongest effect on whether a sample contains BST fossils, with very low probabilities if the mineral is present. Illite composition 2, berthierine/chamosite, and celadonite were also found to be significant determinants of the outcome. The technique also identified a range of conditions (pathway highlighted in red in Fig. 3) which almost always yielded BST fossils (probability = 0.966).

The overall rate of correct classification was high for both models: 79.3% for the logistic regression and 83.1% for the classification tree. Interestingly, both models were better at correctly identifying samples that contain BST fossils than those that do not. The sensitivity (rate of correct classification of rocks that contained BST fossils) ranged between 87.9% and 89.3%, while the specificity (rate of correct classification of the rocks that contained only fossil mineralized skeletons) was between 63.4% and 75.6%.

DISCUSSION AND CONCLUSIONS

The data presented here provide the first statistical evidence of an association between the clay mineralogy of sedimentary rocks and the presence of macroscopic Cambrian BST fossils, providing a mineralogical fingerprint that can be used to refine the search for these crucial fossil assemblages and provide insight into the conditions conducive to fossilization. Whereas previous hypotheses for the influence of sediment-hosted clay minerals on BST fossilization emphasized detrital mineralogy (Butterfield,

159 1990, 1995; Wilson and Butterfield, 2014; Naimark et al., 2016a; Naimark et al., 2016b),
160 the only mineral identified in this study as increasing the chances of a sample containing
161 BST fossils, berthierine/chamosite, forms during early diagenesis via the transformation
162 of structurally analogous kaolinite (which may have been detrital in source) in the
163 presence of pore-water iron (Fe^{2+}) (Bhattacharyya, 1983; Taylor, 1990; Taylor and
164 Curtis, 1995; Fritz and Toth, 1997; Toth and Fritz, 1997; Rivard et al., 2013). A role for
165 this precursor aluminum-rich kaolinite in BST fossilization is supported by experimental
166 data, which emphasize its antibacterial properties and propensity to promote BST
167 fossilization via polymerization of organic molecules (Wilson and Butterfield, 2014;
168 McMahon et al., 2016; Naimark et al., 2016a; Naimark et al., 2016b). Berthierine and the
169 free iron required for its formation may have had similar effects (Petrovich, 2001; Wilson
170 and Butterfield, 2014; McMahon et al., 2016). Our data suggest that almost complete
171 transformation of kaolinite has occurred as this mineral is essentially absent in our
172 samples. Following conversion to berthierine/chamosite any remaining kaolinite was
173 likely lost during later (burial) diagenesis to illite phases (see GSA Data Repository). As
174 Cambrian anoxic water masses were commonly ferruginous (Sperling et al., 2015) some
175 portion of the iron required for this transformation may have been supplied from
176 seawater. However, independent evidence from sulfur isotopes suggests that diffusion of
177 ions into BST fossil-bearing sediments was restricted early in diagenesis, possibly
178 reflecting “closed system” conditions brought about by early carbonate cements (Gaines
179 et al., 2012; Hammarlund et al., 2017). Fe^{2+} generated by microbial reduction of iron-
180 oxides and oxyhydroxides in sediment is typically released to anoxic bottom waters
181 (Elrod et al., 2004) but closed system conditions would have promoted the retention of

182 Fe^{2+} , and increased the time available for the transformation of kaolinite to
183 berthierine/chamosite. The high berthierine abundance within Cambrian BST fossil-
184 bearing strata might be accounted for not only by distinct diagenetic conditions but also
185 by paleogeographic/climatic factors. Kaolinite is generated through chemical weathering
186 in tropical environments where drainage is high and soil pH is low (Wilson, 2013): these
187 environments have high kaolinite/smectite ratios (although smectite is absent in our
188 samples, it is likely represented by its burial product illite which has a strong negative
189 effect on the presence of BST fossils). Cambrian BST fossil-bearing localities are
190 concentrated in tropical paleolatitudes (e.g., Hendricks et al., 2008).

191 Other hypotheses relating sediment composition to BST fossilization are not
192 supported by our results. For example, montmorillonite has been posited to slow decay
193 prior to fossilization by adsorbing autolytic enzymes (Butterfield, 1990, 1995; but see
194 Wilson and Butterfield, 2014), but it is not abundant in samples hosting BST fossils.
195 Although some of the illite identified in our samples may have formed through illitization
196 of smectite, the strong negative correlation between illite and samples containing BST
197 fossils implies that smectite was not conducive to preservation (Wilson and Butterfield,
198 2014). Previous studies observed a relationship between the occurrence of glauconite and
199 BST fossil-bearing localities (e.g., Aitken et al., 1973; Odom, 1976; Rolf et al., 1977;
200 Butterfield, 1994; Butterfield and Harvey, 2012; Wilson and Butterfield, 2014), however
201 the abundance of glauconite is not significantly higher in samples that contain BST
202 fossils (see GSA Data Repository).

203 Although mineralogy is an important predictor of macroscopic Cambrian BST
204 fossilization (and berthierine/chamosite and kaolinite may play a role through their

antibacterial/polymerization properties), it cannot be the only factor involved in the process: the area occupied by samples with BST fossils in the PCoA plot (Fig. 1) overlaps in large part the area occupied by samples that only yield mineralized skeletons. Other factors may include rapid burial, marine anoxia, and the role of authigenic mineralization in sealing sedimentary layers containing fossils and in mineralizing certain tissues (see Gaines, 2014 for review). However, our mineralogical data indicate that a unique combination of diagenetic and paleogeographic/climatic factors may account for the high abundance of Cambrian BST fossil-bearing deposits (Muscente et al., 2017). They also provide a mineralogical search-image for strata likely to preserve BST fossils, which may allow more efficient prospecting of successions and potentially facilitate the exploration of other planets such as Mars for evidence of past life.

ACKNOWLEDGMENTS

Financial support was provided by the Leverhulme Trust (PLP-2015-286), the NASA Astrobiology Institute (NNA13AA90A), a NASA Earth and Space Science Fellowship (NNX14AP10H), the National Science Foundation (NSF EAR-1554897), and the Yale Institute for Biospheric Studies and Peabody Museum. A. Barroll assisted in sample analysis. S. Butts, J. Utrup, D. Siveter, E. Howlett, and J. Hay facilitated access to collections. We thank G. Budd, N. Butterfield, and an anonymous reviewer for helpful comments.

REFERENCES CITED

Aitken, J.D., Macqueen, R.W., and Usher, J.L., 1973, Reconnaissance studies of Proterozoic and Cambrian stratigraphy, lower Mackenzie River area: District of Mackenzie: Geological Survey of Canada Papers, v. 73, p. 1–163.

- 228 Bhattacharyya, D.P., 1983, Origin of berthierine in ironstones: *Clays and Clay Minerals*,
229 v. 31, p. 173–182, <https://doi.org/10.1346/CCMN.1983.0310302>.
- 230 Butterfield, N.J., 1990, Organic preservation of non-mineralizing organisms and the
231 taphonomy of the Burgess Shale: *Paleobiology*, v. 16, p. 272–286,
232 <https://doi.org/10.1017/S0094837300009994>.
- 233 Butterfield, N.J., 1994, Burgess Shale-type fossils from a Lower Cambrian shallow-shelf
234 sequence in northwestern Canada: *Nature*, v. 369, p. 477–479,
235 <https://doi.org/10.1038/369477a0>.
- 236 Butterfield, N.J., 1995, Secular distribution of Burgess-Shale-type preservation: *Lethaia*,
237 v. 28, p. 1–13, <https://doi.org/10.1111/j.1502-3931.1995.tb01587.x>.
- 238 Butterfield, N.J., and Harvey, T.H.P., 2012, Small carbonaceous fossils (SCFs): A new
239 measure of early Paleozoic paleobiology: *Geology*, v. 40, p. 71–74,
240 <https://doi.org/10.1130/G32580.1>.
- 241 Caron, J.-B., and Jackson, D.A., 2006, Taphonomy of the greater Phyllopod Bed
242 community, Burgess Shale: *Palaaios*, v. 21, p. 451–465,
243 <https://doi.org/10.2110/palo.2003.P05-070R>.
- 244 Cohen, P.A., and Macdonald, F.A., 2015, The Proterozoic record of eukaryotes:
245 *Paleobiology*, v. 41, p. 610–632, <https://doi.org/10.1017/pab.2015.25>.
- 246 Conway Morris, S., 1986, The community structure of the Middle Cambrian Phyllopod
247 Bed (Burgess Shale): *Palaeontology*, v. 29, p. 423–467.
- 248 Curtin, L.G., and Gaines, R.R., 2011, Burges Shale-type preservation and detrital clay
249 mineralogy: A test of the “reactive clay” hypothesis: *Geological Society of America*
250 *Abstracts with Programs*, v. 43, no. 5, p. 108.

- 251 Elrod, V.A., Berelson, W.M., Coale, K.H., and Johnson, K.S., 2004, The flux of iron
252 from continental shelf sediments: A missing source for global budgets: *Geophysical*
253 *Research Letters*, v. 31, L12307, <https://doi.org/10.1029/2004GL020216>.
- 254 Forchielli, A., Steiner, M., Kasbohm, J., Hu, S., and Keupp, H., 2014, Taphonomic traits
255 of clay-hosted early Cambrian Burgess Shale-type fossil Lagerstätten in South
256 China: *Palaeogeography, Palaeoclimatology, Palaeoecology*, v. 398, p. 59–85,
257 <https://doi.org/10.1016/j.palaeo.2013.08.001>.
- 258 Fritz, S.J., and Toth, T.A., 1997, An Fe-berthierine from a Cretaceous laterite: Part II.
259 Estimation of Eh, pH, and pCO₂ conditions of formation: *Clays and Clay Minerals*,
260 v. 45, p. 580–586, <https://doi.org/10.1346/CCMN.1997.0450409>.
- 261 Gaines, R.R., 2014, Burgess Shale-type preservation and its distribution in space and
262 time: *Paleontological Society Papers*, v. 20, p. 123–146.
- 263 Gaines, R.R., Hammarlund, E.U., Hou, X., Qi, C., Gabbott, S.E., Zhao, Y., Peng, J., and
264 Canfield, D.E., 2012, Mechanism for Burgess Shale-type preservation: *Proceedings*
265 *of the National Academy of Sciences of the United States of America*, v. 109,
266 p. 5180–5184, <https://doi.org/10.1073/pnas.1111784109>.
- 267 Gaines, R.R., Mering, J.A., Zhao, Y., and Peng, J., 2011, Stratigraphic and microfacies
268 analysis of the Kaili Formation, a candidate GSSP for the Cambrian Series 2-Series 3
269 boundary: *Palaeogeography, Palaeoclimatology, Palaeoecology*, v. 311, p. 171–183,
270 <https://doi.org/10.1016/j.palaeo.2011.08.018>.
- 271 Hammarlund, E.U., Gaines, R.R., Prokopenko, M.G., Qi, C., Hou, X., and Canfield, D.E.,
272 2017, Early Cambrian oxygen minimum zone-like conditions at Chengjiang: *Earth*

- 273 and Planetary Science Letters, v. 475, p. 160–168,
274 <https://doi.org/10.1016/j.epsl.2017.06.054>.
- 275 Hendricks, J.R., Lieberman, B.S., and Stigall, A.L., 2008, Using GIS to study
276 palaeobiogeographic and macroevolutionary patterns in soft-bodied Cambrian
277 arthropods: Palaeogeography, Palaeoclimatology, Palaeoecology, v. 264, p. 163–
278 175, <https://doi.org/10.1016/j.palaeo.2008.04.014>.
- 279 Hornibrook, E.R.C., and Longstaffe, F.J., 1996, Berthierine from the Lower Cretaceous
280 Clearwater Formation, Alberta, Canada: Clays and Clay Minerals, v. 44, p. 1–21,
281 <https://doi.org/10.1346/CCMN.1996.0440101>.
- 282 McMahon, S., Anderson, R.P., Saupe, E.E., and Briggs, D.E.G., 2016, Experimental
283 evidence that clay inhibits bacterial decomposers: Implications for preservation of
284 organic fossils: Geology, v. 44, p. 867–870, <https://doi.org/10.1130/G38454.1>.
- 285 Muscente, A.D., et al., 2017, Exceptionally preserved fossil assemblages through
286 geologic time and space: Gondwana Research, v. 48, p. 164–188,
287 <https://doi.org/10.1016/j.gr.2017.04.020>.
- 288 Naimark, E., Kalinina, M., Shokurov, A., Boeva, N., Markov, A., and Zaytseva, L.,
289 2016a, Decaying in different clays: Implications for soft-tissue preservation:
290 Palaeontology, v. 59, p. 583–595, <https://doi.org/10.1111/pala.12246>.
- 291 Naimark, E.B., Kalinina, M.A., Shokurov, A.V., Markov, A.V., and Boeva, N.M., 2016b,
292 Decaying of *Artemia salina* in clay colloids: 14-month experimental formation of
293 subfossils: Journal of Paleontology, v. 90, p. 472–484,
294 <https://doi.org/10.1017/jpa.2016.23>.

- 295 Odom, I.E., 1976, Microstructure, mineralogy and chemistry of Cambrian glauconite
296 pellets and glauconite, central USA: *Clays and Clay Minerals*, v. 24, p. 232–238,
297 <https://doi.org/10.1346/CCMN.1976.0240504>.
- 298 Petrovich, R., 2001, Mechanisms of fossilization of the soft-bodied and lightly armored
299 faunas of the Burgess Shale and of some other classical localities: *American Journal*
300 *of Science*, v. 301, p. 683–726, <https://doi.org/10.2475/ajs.301.8.683>.
- 301 Powell, W., 2003, Greenschist-facies metamorphism of the Burgess Shale and its
302 implications for models of fossil formation and preservation: *Canadian Journal of*
303 *Earth Sciences*, v. 40, p. 13–25, <https://doi.org/10.1139/e02-103>.
- 304 R Development Core Team, 2016, R: A language and environment for statistical
305 computing: Vienna, Austria, R Foundation for Statistical Computing.
- 306 Rivard, C., Pelletier, M., Michau, N., Razafitianamaharevo, A., Bihannic, I., Abdelmoula,
307 M., Ghanbaja, J., and Villéras, F., 2013, Berthierine-like mineral formation and
308 stability during interaction of kaolinite with metallic iron at 90°C under anoxic and
309 oxic conditions: *The American Mineralogist*, v. 98, p. 163–180,
310 <https://doi.org/10.2138/am.2013.4073>.
- 311 Rolf, R.M., Kimball, C.W., and Odom, I.E., 1977, Mössbauer characteristics of Cambrian
312 glauconite, central USA: *Clays and Clay Minerals*, v. 25, p. 131–137,
313 <https://doi.org/10.1346/CCMN.1977.0250210>.
- 314 Snyder, R.L., and Bish, D.L., 1989, Quantitative analysis: *Reviews in Mineralogy and*
315 *Geochemistry*, v. 20, p. 101–144.
- 316 Sperling, E.A., Wolock, C.J., Morgan, A.S., Gill, B.C., Kunzmann, M., Halverson, G.P.,
317 Macdonald, F.A., Knoll, A.H., and Johnston, D.T., 2015, Statistical analysis of iron

geochemical data suggests limited late Proterozoic oxygenation: *Nature*, v. 523,
p. 451–454, <https://doi.org/10.1038/nature14589>.

Środoń, J., Drits, V.A., McCarty, D.K., Hsieh, J.C.C., and Eberl, D.D., 2001,

Quantitative X-ray diffraction analysis of clay-bearing rocks from random
preparations: *Clays and Clay Minerals*, v. 49, p. 514–528,
<https://doi.org/10.1346/CCMN.2001.0490604>.

Taylor, K.G., 1990, Berthierine from the non-marine Wealden (Early Cretaceous)

sediments of south-east England: *Clay Minerals*, v. 25, p. 391–399,
<https://doi.org/10.1180/claymin.1990.025.3.13>.

Taylor, K.G., and Curtis, C.D., 1995, Stability and facies association of early diagenetic

mineral assemblages: An example from a Jurassic ironstone-mudstone succession,
UK: *Journal of Sedimentary Research*, v. 65, p. 358,
<https://doi.org/10.1306/D42680C2-2B26-11D7-8648000102C1865D>.

Toth, T.A., and Fritz, S.J., 1997, An Fe-berthierine from a Cretaceous laterite: Part I.

Characterization: *Clays and Clay Minerals*, v. 45, p. 564–579,
<https://doi.org/10.1346/CCMN.1997.0450408>.

Wilson, L.A., and Butterfield, N.J., 2014, Sediment effects on the preservation of

Burgess Shale-type compression fossils: *Palaios*, v. 29, p. 145–154,
<https://doi.org/10.2110/palo.2013.075>.

Wilson, M.J., 2013, 3C: Clay minerals, in Deer, W.A., et al., *Rock Forming Minerals*:

London, The Geological Society of London, 724 p.

FIGURE CAPTIONS

341

342 Figure 1. Principal coordinate (PCoA) ordination plot showing the variation in clay
343 mineralogy among samples (dots) in two-dimensional space. Samples that contain
344 Burgess Shale-type (BST) fossils (red) are distinguished from those that contain only
345 fossil mineralized skeletons (blue). Frequency distributions of samples are plotted on
346 each axis. Convex hulls delimit the space explored by both classes of samples, and
347 centroids are plotted as diamonds.

348

349 Figure 2. Multiple logistic regression model obtained through stepwise variable selection
350 coupled with LRT. Individual plots show the effect of the abundance of a given clay
351 mineral on the probability of a sample containing BST fossils. Grey area indicates 95%
352 confidence interval.

353

354 Figure 3. Conditional inference classification tree showing optimal subdivision of the
355 data. Numbers above tree branches show the values for the binary splits. Size and
356 composition of subsets are given below, with colors as in Figure 1.

357

358 1GSA Data Repository item 2018xxx comprising further details of methodology
359 including statistical methods, sensitivity tests, further discussion of the origin of the clay
360 assemblage, frequency distributions of XRD d-spacings, correlation matrix of clay
361 abundance, and data table, is available online at
362 <http://www.geosociety.org/datarepository/2018/> or on request from
363 editing@geosociety.org.

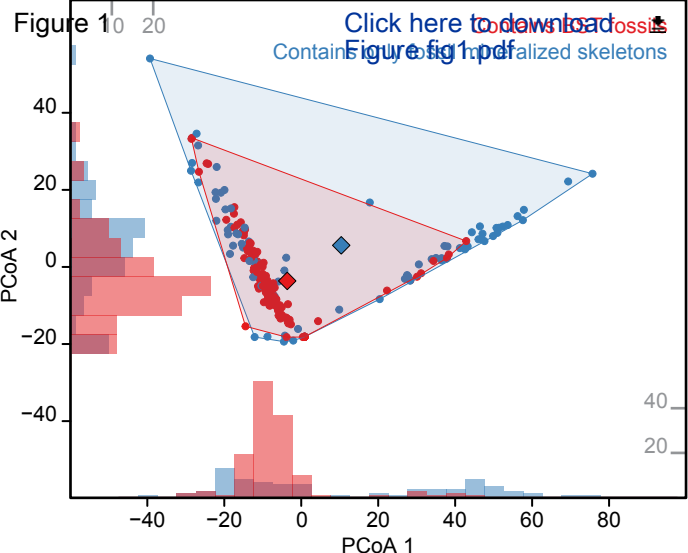
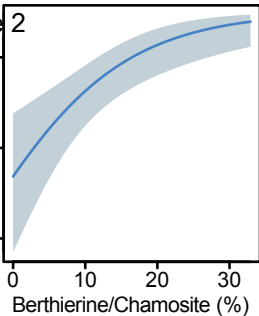


Figure 2

Probability sample contains BST fossils



[Click here to download Figure fig2.pdf](#)

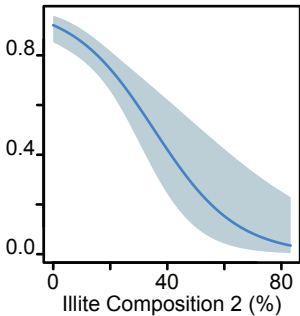
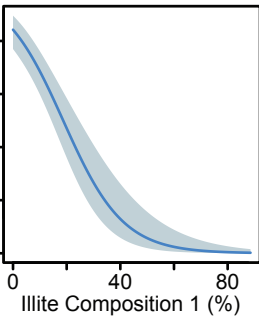
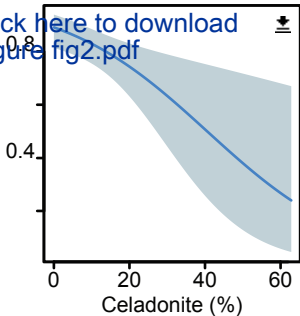
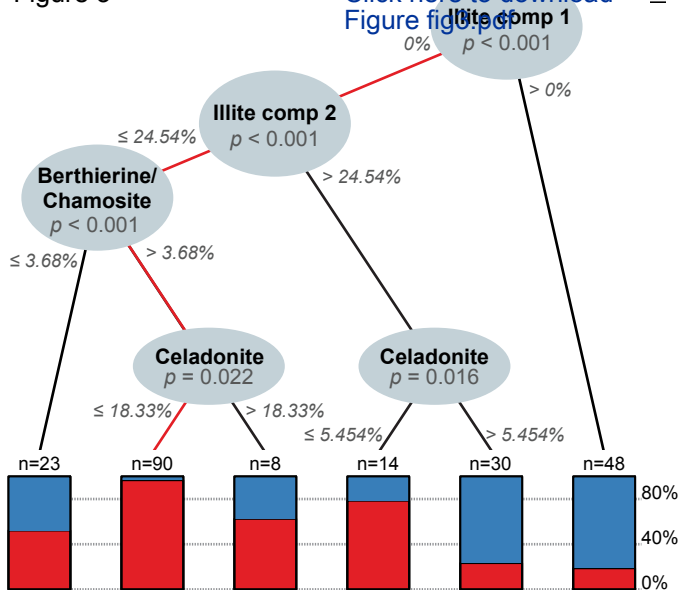


Figure 3

[Click here to download Figure figure.pdf](#)



GSA Data Repository

A mineralogical signature for Burgess Shale-type fossilization

Ross P. Anderson, Nicholas J. Tosca, Robert R. Gaines, Nicolás Mongiardino Koch, and Derek E.G. Briggs

Email: ross.anderson@all-souls.ox.ac.uk

Further methodological particulars

Samples were taken from the collections of R.R. Gaines (n = 184), the Oxford University Museum of Natural History (n = 11), and the Yale Peabody Museum of Natural History (n = 18).

Matrix material was selected randomly from that immediately surrounding (i.e., within a few centimeters) the fossil (in the case of museum specimens), or from the same bed as fossiliferous material (in the case of specimens in the collection of R.R. Gaines). Samples from which BST fossils are considered absent were selected from localities where significant collection efforts have revealed no soft-bodied fossils in these particular horizons. Although absence of recovered BST fossils does not provide absolute evidence of their absence from these horizons, we compared these samples to many others in our dataset in which soft bodied fossils are conspicuous and abundant. Material was hand-ground to approximately 10 μm grain size with a porcelain pestle and mortar. Enough matrix material was ground to adequately cover single silicon crystal substrates 27 mm in diameter.

All X-ray diffraction (XRD) peak positions were adjusted to correct for slight variations in sample height displacement error using positions of quartz reflections as internal standards. Analysis of the 060 region identified other peaks in the range 1.520–1.530 \AA , but their abundance was positively correlated with that of calcite obtained from the bulk analysis, consistent with the identification of variable quantities of this mineral through bulk analysis (Kendall's $\tau = 0.6344$, $P < 10^{-16}$). Additional confirmation of clay mineral species were obtained through analysis of oriented $< 2 \mu\text{m}$ clay separates. Such separates were analyzed from 22 samples representing the entire suite of clay minerals observed, in order to ensure consistency in clay mineral identification with the 060 powder analysis. The mineral identifications were consistent between the two methods.

Statistical methodology

Abundance of all clay minerals showed a highly skewed zero-inflated distribution, resulting in a departure from multivariate normality, and most pairs of clay minerals proved to be significantly correlated (Fig. S2). We therefore transformed the dataset to a matrix of pair-wise Euclidean distances between observations, and we used principal coordinate analysis (PCoA) to visualize the variability. Differences in clay mineral composition between samples with BST fossils and those with only fossil mineralized skeletons were tested using PERMANOVA (Anderson, 2001). Differences in the multivariate spread of both groups were tested using permutational analysis of multivariate dispersion, hereafter PERMDISP (Anderson, 2006). Both analyses were implemented using the package *vegan* (Oksanen et al., 2016), and significance was evaluated by performing 10^5 permutations.

We performed a multiple logistic regression to investigate how different clay minerals affected the probability of samples containing BST fossils. This regression used the six clay mineral abundance variables as predictors of a binary outcome: the presence of BST fossils or the presence of only fossil mineralized skeletons. The best fitting logistic model was determined using stepwise variable selection in both directions. At each step, the inclusion or exclusion of any given predictor from the model was assessed using likelihood ratio tests (LRT). The best fitting model was visualized with the package *visreg* (Breheny and Burchett, 2016).

Finally, the relationship between clay mineral composition and BST fossil-bearing samples was explored using a conditional inference classification tree (Strobl et al., 2009) built using the package *partykit* (Hothorn and Zeileis, 2015). This approach selects the predictor with the strongest association with the response variable (using Bonferroni adjusted P values), implements a binary split, and iterates over the newly generated subsets of data until the null hypothesis of independence cannot be rejected (Hothorn et al., 2006). This procedure guarantees unbiased variable selection and avoids overfitting (Hothorn and Zeileis, 2015).

The goodness of fit of the models derived from these two approaches (logistic regression and classification tree) was evaluated based on classification accuracy.

Independence of samples

The statistical models are all based on the assumption that each observation is independent. Many of our samples derive from stratigraphic suites from the same geological formation and locality. Clay mineral assemblages are controlled in part by the provenance of detrital clay input into a geological basin over time, and the impact of diagenesis on that detrital assemblage. Thus the possibility that clay composition could be similar in samples from the same succession must be taken into account in interpreting the significance of the results presented here. Where multiple samples were taken from the same formation, each distinct horizon is represented by just one sample. All samples therefore derive from different depositional events, which reduces the expected dependence between samples. Furthermore, methods accommodating some lack of independence among observations from the same locality were also tested whenever possible. We ran the multiple logistic regression model using the Huber-White method (Huber, 1967; White, 1982), which adjusts the variance-covariance matrix to correct for correlated responses from clustered samples (Cameron and Miller, 2015), with formation provenance as clustering variable. This analysis supported the same results ($P \leq 0.0001$ for illite composition 1 and illite composition 2, 0.0023 for berthierine/chamosite and 0.029 for celadonite). Thus the stratigraphic bundling of a proportion of the samples does not compromise our conclusions regarding the effect of clay minerals on organic preservation.

Absolute abundances of clays

Obtaining the absolute abundance of clay minerals within a given sample is challenging. While quantitative data can be obtained using Rietveld refinement (Snyder and Bish, 1989), such a procedure is not feasible on a sample set of this size. To obtain semi-quantitative estimates of abundances we scaled the relative clay mineral proportions from the 060 region to the total clay fraction from the bulk mineralogical analysis. This total fraction was determined by summing all identified clay mineral abundances in the bulk results and, for selected samples, checking this relationship against the total integrated area of the 020 reflection, common to all layer silicates (Środoń et al., 2001). This technique preserved the relative differences in clay content between samples.

The influence of diagenetic carbonate minerals on statistical models

There is evidence that carbonate minerals in many of these rocks are a product of early diagenesis (e.g., Gaines et al., 2012). We removed both calcite and dolomite from the mineralogical data and adjusted the abundances of the other minerals accordingly, in an attempt to better represent the original (pre-diagenetic) mineralogical composition of the samples. The

results remain robust to this adjustment: the logistic regression model is almost identical, including significant effects of illite composition 1, illite composition 2, berthierine/chamosite, and celadonite ($P = 2.2e^{-12}$, $9.4e^{-7}$, $4.8e^{-4}$, and $2.6e^{-3}$, respectively), as well as a marginally significant effect of glauconite ($P = 0.046$). Kaolinite has no effect ($P = 0.14$).

The influence of illite composition 1 and the Kaili Formation on statistical models

The abundance of illite composition 1 is a crucial factor in distinguishing samples that contain BST fossils from those that contain only fossil mineralized skeletons. Not only is it recovered by both models as the most important predictor of association with carbonaceous fossils, it is also significantly negatively correlated with the abundance of all other clay minerals (Fig. S2). The Kaili Formation, which represents 22% of our entire dataset, is especially rich in illite composition 1, with a mean abundance of 37.9% (standard deviation = 22.8%) compared to only 2.05% (standard deviation = 10.36%) in all other samples. In order to test whether the samples from the Kaili Formation bias our results, we ran the multiple logistic regression without them. The results are robust to the removal of Kaili samples. Not only did illite composition 1 remain the most significant predictor of whether a sample would contain BST fossils, the model supported was identical, including illite composition 2, celadonite, and berthierine/chamosite ($P = 2.2e^{-6}$, $1.9e^{-7}$, $5.0e^{-3}$ and $2.4e^{-2}$, respectively). No significant effect of glauconite or kaolinite was detected ($P = 0.26$ and 0.34 , respectively).

Origin of the observed clay mineral assemblage

The composition of the observed clay mineral assemblages depends on the original detrital material and the degree to which it has been transformed in response to pore water chemistry during early and/or late diagenesis (including burial metamorphism). Thus, clay mineral assemblages are prone to alteration by weathering. In fine-grained siliciclastic rocks, the mineral most susceptible to weathering is pyrite, which if chemically altered could mobilize iron and might lead to secondary precipitation of Fe-minerals such as berthierine. But Fe-oxides, and jarosite in particular, which are the major products of pyrite weathering, are absent from our samples. Kaolinite, however, is conspicuously absent even though many of these rocks were deposited at tropical paleolatitudes, further supporting a diagenetic origin for berthierine through kaolinite conversion during early and/or late diagenesis (e.g., Bhattacharyya, 1983; Taylor, 1990; Taylor and Curtis, 1995; Fritz and Toth, 1997; Toth and Fritz, 1997; Rivard et al., 2013). Where berthierine has been reported from laterites rich in kaolinite and Fe-oxides (e.g., Toth and Fritz, 1997 and references therein), these laterites have been drowned by marine transgressions, or stagnant groundwater flow has led to reductive diagenetic transformation of goethite and kaolinite to berthierine. Berthierine is not a product of the chemical weathering process *sensu stricto*, but a product derived from the reaction between Fe^{2+} and kaolinite (i.e., Bhattacharyya, 1983). This relationship also explains why the major occurrence of berthierine is in ironstones, where it alternates with glauconite as an authigenic cement (Pufahl, 2010). The diagenetic transformation of kaolinite in the presence of Fe^{2+} drives this process (demonstrated in the laboratory by Bhattacharyya, 1983): goethite and kaolinite are dominant detrital components of the tropical soils that generate the ironstones (Pufahl, 2010). We therefore do not consider weathering to have compromised our data in a significant manner, particularly in relation to the formation of berthierine.

References

- Anderson, M. J., 2001, A new method for non-parametric multivariate analysis of variance: *Austral Ecology*, v. 26, no. 1, p. 32–46.
- Anderson, M. J., 2006, Distance-based tests for homogeneity of multivariate dispersions: *Biometrics*, v. 62, no. 1, p. 245–253.
- Bhattacharyya, D. P., 1983, Origin of berthierine in ironstones: *Clays and Clay Minerals*, v. 31, no. 3, p. 173–182.
- Breheny, P., and Burchett, W., 2016, Visualization of Regression Models using visreg.
- Cameron, A. C., and Miller, D. L., 2015, A practitioner's guide to cluster-robust inference: *Journal of Human Resources*, v. 50, no. 2, p. 317–372.
- Fritz, S. J., and Toth, T. A., 1997, An Fe-berthierine from a Cretaceous laterite: Part II. Estimation of Eh, pH, and pCO₂ conditions of formation: *Clays and Clay Minerals*, v. 45, no. 4, p. 580–586.
- Gaines, R. R., Hammarlund, E. U., Hou, X., Qi, C., Gabbott, S. E., Zhao, Y., Peng, J., and Canfield, D. E., 2012, Mechanism for Burgess Shale-type preservation: *Proceedings of the National Academy of Sciences*, v. 109, no. 14, p. 5180–5184.
- Hothorn, T., Hornik, K., and Zeileis, A., 2006, Unbiased recursive partitioning: A conditional inference framework: *Journal of Computational and Graphical statistics*, v. 15, no. 3, p. 651–674.
- Hothorn, T., and Zeileis, A., 2015, partykit: A modular toolkit for recursive partytioning in R: *Journal of Machine Learning Research*, v. 16, p. 3905–3909.
- Huber, P. J., 1967, The behaviour of maximum likelihood estimates under nonstandard conditions: *Proceedings of the fifth Berkeley symposium on mathematical statistics and probability*, p. 221–233.
- Oksanen, J., Blanchet, F. G., Kindt, R., Legendre, P., Minchin, P. R., O'Hara, R. B., Simpson, G. L., Solymos, P., Stevens, M. H. H., and Wagner, H., 2016, vegan: Community Ecology Package.
- Pufahl, P. K., 2010, Bioelemental sediments, Facies models 4, Volume 6, Geological Association of Canada GEOText, p. 477–503.
- Rivard, C., Pelletier, M., Michau, N., Razafitianamaharevo, A., Bihannic, I., Abdelmoula, M., Ghanbaja, J., and Villéras, F., 2013, Berthierine-like mineral formation and stability during interaction of kaolinite with metallic iron at 90°C under anoxic and oxic conditions: *American Mineralogist*, v. 98, no. 1, p. 163–180.
- Snyder, R. L., and Bish, D. L., 1989, Quantitative analysis: *Reviews in Mineralogy and Geochemistry*, v. 20, no. 1, p. 101–144.
- Środoń, J., Drits, V. A., McCarty, D. K., Hsieh, J. C. C., and Eberl, D. D., 2001, Quantitative X-ray diffraction analysis of clay-bearing rocks from random preparations: *Clays and Clay Minerals*, v. 49, no. 6, p. 514–528.
- Strobl, C., Malley, J., and Tutz, G., 2009, An introduction to recursive partitioning: rationale, application, and characteristics of classification and regression trees, bagging, and random forests: *Psychological Methods*, v. 14, no. 4, p. 323.
- Taylor, K. G., 1990, Berthierine from the non-marine Wealden (Early Cretaceous) sediments of south-east England: *Clay Minerals*, v. 25, no. 3, p. 391–399.
- Taylor, K. G., and Curtis, C. D., 1995, Stability and facies association of early diagenetic mineral assemblages: An example from a Jurassic ironstone-mudstone succession, UK: *Journal of Sedimentary Research*, v. 65, no. 2a, p. 358–368.

- Toth, T. A., and Fritz, S. J., 1997, An Fe-berthierine from a Cretaceous laterite: Part I. Characterization: *Clays and Clay Minerals*, v. 45, no. 4, p. 564–579.
- White, H., 1982, Maximum likelihood estimation of misspecified models: *Econometrica: Journal of the Econometric Society*, p. 1–25.

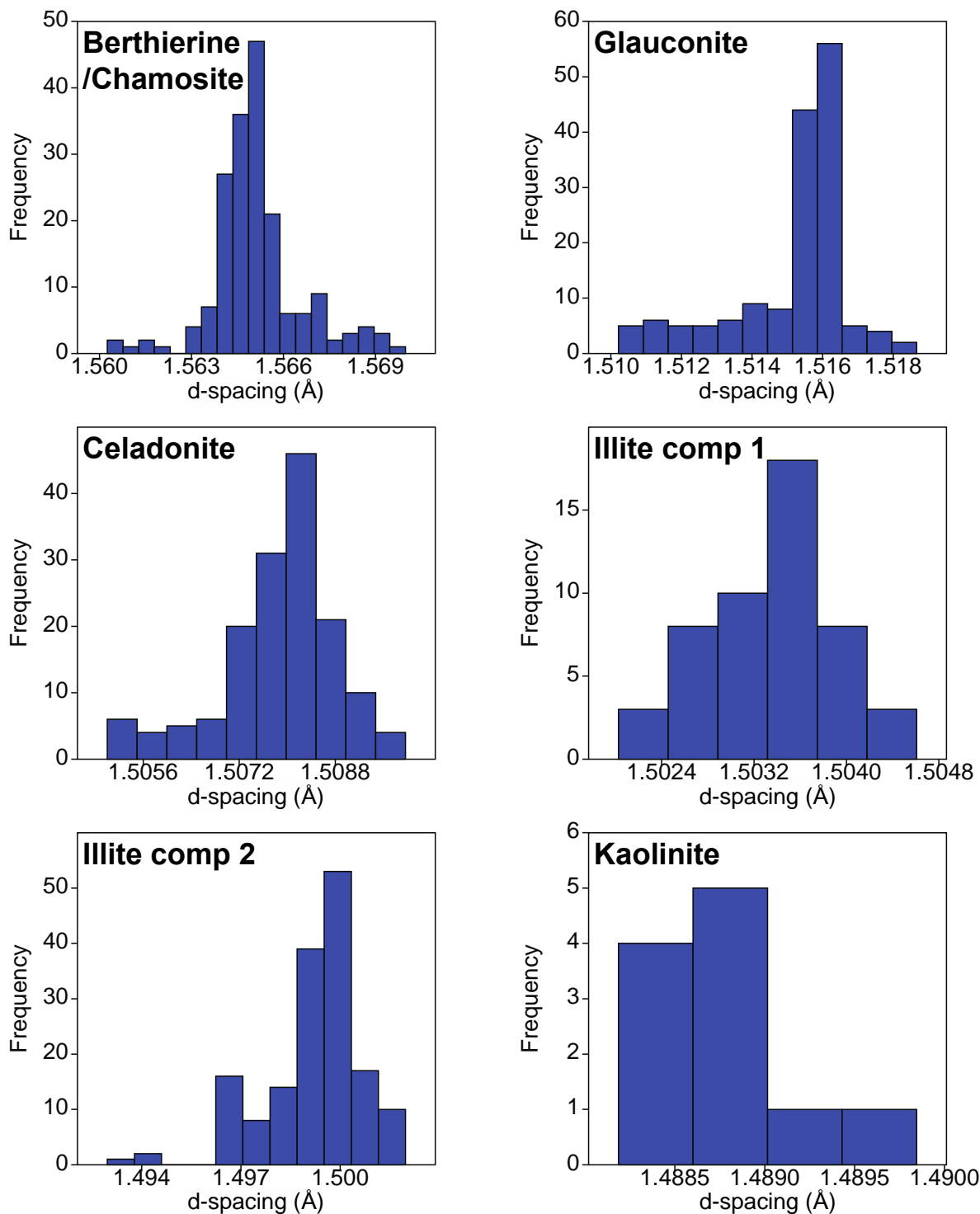


Figure S1: Frequency distributions of d-spacing for 060 peaks of berthierine/chamosite (1.560–1.570 Å), glauconite (1.510–1.519 Å), celadonite (1.505–1.510 Å), illite composition 1 (1.502–1.505 Å), illite composition 2 (1.493–1.502 Å), and kaolinite (~1.489 Å).

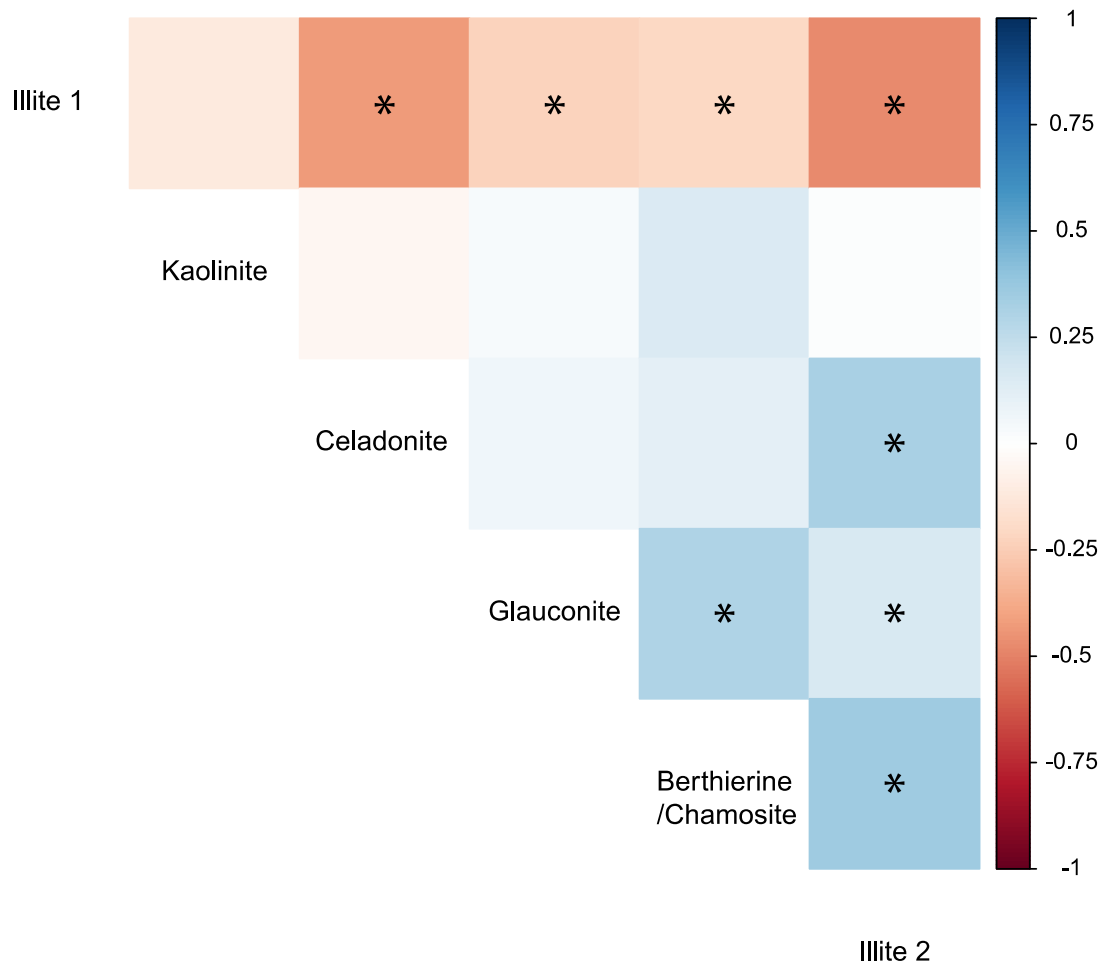


Figure S2: Correlation matrix for the abundance of clay minerals included in the analysis. Grid colors represent Kendall's τ , and significant levels of correlation after applying Bonferroni correction are marked with an asterisk. Severe correlation between predictor variables (multicollinearity) can influence the results of a logistic regression by inflating the standard errors of the coefficients. Nonetheless, our dataset shows only moderate levels of multicollinearity which should not have a strong impact on the results (variance inflation factors for all variables ≤ 1.56).

Sample Name	Country	Stratigraphy				Contains BST fossils	Composition (% rock)								
		Formation	Member	Sequence	Height		Qtz	Calc	Dol	Bth	Gl	Cel	Il 1	Il 2	Kaol
CMj SG 0.85	USA	Marjum		Sponge Gulch	0.85	Y	34.0	22.0		9.0	5.1	11.0	0.0	7.9	0.0
CMj SG 0.93	USA	Marjum		Sponge Gulch	0.93	Y	32.0	18.0		15.6	8.9	14.1	0.0	11.4	0.0
CMj SG 0.98	USA	Marjum		Sponge Gulch	0.98	Y	36.0	25.0		9.4	5.1	13.0	0.0	10.5	0.0
CMj RW 1.26	USA	Marjum		Red Cliffs Wash	1.26	Y	31.0	19.0		7.0	7.7	18.0	0.0	15.3	0.0
CMj RW 1.28	USA	Marjum		Red Cliffs Wash	1.28	Y	32.0	17.0		8.0	5.2	16.5	0.0	18.3	0.0
CMj RW 1.38	USA	Marjum		Red Cliffs Wash	1.38	Y	30.0	14.0		7.5	7.0	15.6	0.0	16.9	0.0
CMj RW 1.44	USA	Marjum		Red Cliffs Wash	1.44	Y	28.0	12.0	4.0	8.3	4.3	17.3	0.0	19.2	0.0
CMj RW 1.82	USA	Marjum		Red Cliffs Wash	1.82	Y	25.0	16.0	5.0	6.4	8.9	15.0	0.0	19.7	0.0
CMj RW 1.92	USA	Marjum		Red Cliffs Wash	1.92	Y	41.0	8.0	8.0	10.9	2.8	7.8	0.0	14.4	0.0
CMj RW 1.96	USA	Marjum		Red Cliffs Wash	1.96	Y	34.0	9.0	8.0	7.6	3.2	8.7	0.0	21.5	0.0
CMj WHQ 1	USA	Marjum		White Hill Quarry	1.00	Y	22.0	15.0		13.3	7.3	14.2	0.0	12.2	0.0
CMj WHQ 2	USA	Marjum		White Hill Quarry	2.00	Y	37.0	21.0		6.7	7.1	11.8	0.0	9.4	0.0
CMj WHQ 3	USA	Marjum		White Hill Quarry	3.00	Y	25.0	24.0		9.4	8.5	14.0	0.0	9.1	0.0
CMj WHQ 4	USA	Marjum		White Hill Quarry	4.00	Y	23.0	25.0		10.4	9.8	12.4	0.0	9.4	0.0
CMj WHQ 5	USA	Marjum		White Hill Quarry	5.00	Y	24.0	19.0		13.0	9.6	11.8	0.0	8.5	0.0
CMj KK 7	USA	Marjum		Kell's Knolls	7.00	Y	29.0	6.0		18.2	8.8	12.2	0.0	14.8	0.0
CMj KK 9	USA	Marjum		Kell's Knolls	9.00	Y	25.0	5.0		17.5	7.1	12.0	0.0	14.5	0.0
CMj KK 11	USA	Marjum		Kell's Knolls	11.00	Y	28.0	6.0		17.5	6.1	20.4	0.0	13.0	0.0
CMj KK 13	USA	Marjum		Kell's Knolls	13.00	Y	32.0	10.0		19.2	5.7	18.3	0.0	6.8	0.0
CMj KK 16	USA	Marjum		Kell's Knolls	16.00	Y	30.0	7.0		18.5	4.9	13.5	0.0	13.1	0.0
CMj KK 18	USA	Marjum		Kell's Knolls	18.00	Y	34.0	8.0		24.8	1.0	21.6	0.0	10.7	0.0
CMj KK 20	USA	Marjum		Kell's Knolls	20.00	Y	26.0	7.0		15.0	9.5	15.3	0.0	18.1	0.0
CMj KK 24	USA	Marjum		Kell's Knolls	24.00	Y	41.0	21.0		13.2	6.1	8.2	0.0	9.6	0.0
CMj MPP 64	USA	Marjum		Marjum Pass	64.00	Y	22.0	9.0		19.3	9.1	13.9	0.0	16.7	0.0
CMj MPP 66	USA	Marjum		Marjum Pass	66.00	Y	32.0	15.0		13.7	7.5	9.2	0.0	9.5	0.0
CMj MPP 68	USA	Marjum		Marjum Pass	68.00	Y	28.0	13.0		9.7	6.0	14.4	0.0	12.9	0.0
CMj MPP 70	USA	Marjum		Marjum Pass	70.00	Y	37.0	14.0		15.2	5.1	18.2	0.0	7.5	0.0
CMj MPP 72	USA	Marjum		Marjum Pass	72.00	Y	37.0	23.0		4.9	5.5	7.4	0.0	5.3	0.0

Sample Name	Country	Stratigraphy				Contains BST fossils	Composition (% rock)								
		Formation	Member	Sequence	Height		Qtz	Calc	Dol	Bth	Gl	Cel	Il 1	Il 2	Kaol
CMj MPP 74	USA	Marjum		Marjum Pass	74.00	Y	41.0	25.0		4.3	5.1	7.5	0.0	5.1	0.0
CW 3	USA	Wheeler		Marjum Pass - Lower	3.00	Y	58.0	12.0	9.0	0.0	0.0	0.0	0.0	0.0	0.0
CW 6	USA	Wheeler		Marjum Pass - Lower	6.00	Y	75.0		14.0	1.6	0.0	0.0	0.0	9.4	0.0
CW 9	USA	Wheeler		Marjum Pass - Lower	9.00	Y	37.0			25.4	15.4	0.0	0.0	22.3	0.0
CW 12	USA	Wheeler		Marjum Pass - Lower	12.00	Y	31.0	13.0	6.0	10.6	3.6	15.3	0.0	19.4	0.0
CW 15	USA	Wheeler		Marjum Pass - Lower	15.00	Y	28.0	43.0	2.0	4.0	6.5	6.0	0.0	3.6	0.0
CW 18	USA	Wheeler		Marjum Pass - Lower	18.00	Y	44.0	15.0		12.0	6.9	10.4	0.0	11.7	0.0
CW 21	USA	Wheeler		Marjum Pass - Lower	21.00	Y	34.0	14.0	2.0	13.8	6.9	10.2	0.0	14.1	0.0
CW 24	USA	Wheeler		Marjum Pass - Lower	24.00	Y	22.0	21.0		16.7	6.0	10.2	0.0	10.2	0.0
CW 27	USA	Wheeler		Marjum Pass - Lower	27.00	Y	1.0	8.0		10.2	0.0	13.0	0.0	57.8	0.0
CW 30	USA	Wheeler		Marjum Pass - Lower	30.00	Y				12.9	0.0	10.4	0.0	49.7	0.0
CW 33	USA	Wheeler		Marjum Pass - Lower	33.00	Y		78.0	7.0	0.0	0.0	0.0	0.0	0.0	0.0
CW 36	USA	Wheeler		Marjum Pass - Lower	36.00	Y	25.0	32.0		12.1	7.4	13.4	0.0	4.2	0.0
CW SSA 5	USA	Wheeler		Swasey Spring - Upper	5.00	Y	37.0	12.0		8.4	4.5	7.7	0.0	8.4	0.0
CW SSA 20	USA	Wheeler		Swasey Spring - Upper	20.00	Y	28.0	8.0	2.0	14.0	4.3	11.2	0.0	13.6	0.0
CW SSA 22	USA	Wheeler		Swasey Spring - Upper	22.00	Y	44.0	6.0		17.9	0.0	25.3	0.0	7.8	0.0
CW SSA 27	USA	Wheeler		Swasey Spring - Upper	27.00	Y	59.0	13.0		5.2	5.7	6.7	0.0	8.4	0.0
CW SSA 30	USA	Wheeler		Swasey Spring - Upper	30.00	Y	40.0	18.0		9.1	4.4	11.1	0.0	5.4	0.0
CW SSA 32	USA	Wheeler		Swasey Spring - Upper	32.00	Y	31.0	22.0		11.3	7.4	11.6	0.0	6.7	0.0
CW SSA 34	USA	Wheeler		Swasey Spring - Upper	34.00	Y	25.0	9.0		13.9	8.8	13.1	0.0	16.2	0.0
CW SSA 107	USA	Wheeler		Swasey Spring - Upper	107.00	Y	35.0	16.0		9.9	9.2	11.3	0.0	8.6	0.0
CW SSA 109	USA	Wheeler		Swasey Spring - Upper	109.00	Y	41.0	29.0		5.0	4.1	8.6	0.0	5.4	0.0

Sample Name	Country	Stratigraphy				Contains BST fossils	Composition (% rock)								
		Formation	Member	Sequence	Height		Qtz	Calc	Dol	Bth	Gl	Cel	Il 1	Il 2	Kaol
CW DMJ 26	USA	Wheeler		Drum Mountains	26.00	Y	25.0	14.0	10.0	18.1	6.1	7.7	0.0	10.1	0.0
CW DMJ 29	USA	Wheeler		Drum Mountains	29.00	Y	14.0	29.0		8.0	7.9	14.3	0.0	5.8	0.0
CW DMJ 33	USA	Wheeler		Drum Mountains	33.00	Y	35.0	13.0		12.7	6.6	8.4	0.0	11.2	0.0
CW DMJ 35	USA	Wheeler		Drum Mountains	35.00	Y	27.0	12.0	5.0	20.1	3.1	8.1	0.0	15.7	0.0
CW DMJ 44	USA	Wheeler		Drum Mountains	44.00	Y	22.0	20.0	5.0	14.4	8.1	15.4	0.0	14.2	0.0
CW DMJ 53	USA	Wheeler		Drum Mountains	53.00	Y	26.0	20.0		14.2	7.2	9.1	0.0	9.5	0.0
CW DMJ 61	USA	Wheeler		Drum Mountains	61.00	Y	29.0	32.0		9.2	0.4	13.8	0.0	5.6	0.0
CW DMJ 73	USA	Wheeler		Drum Mountains	73.00	Y	50.0	18.0		8.2	3.2	9.8	0.0	11.9	0.0
CW DMJ 73	USA	Wheeler		Drum Mountains	73.00	Y	29.0	14.0		13.6	8.9	11.7	0.0	11.7	0.0
CW DMJ 75	USA	Wheeler		Drum Mountains	75.00	Y	27.0	7.0		17.6	5.8	13.4	0.0	17.3	0.0
CK W0	China	Kaili		Wuliu-Zengjiayan	0.00	N	4.0		88.0	0.0	0.0	0.0	0.0	0.0	0.0
CK W2	China	Kaili		Wuliu-Zengjiayan	2.00	N	3.0		97.0	0.0	0.0	0.0	0.0	0.0	0.0
CK W5	China	Kaili		Wuliu-Zengjiayan	5.00	N	13.0	52.0		0.0	13.0	18.4	0.0	1.7	0.0
CK W7	China	Kaili		Wuliu-Zengjiayan	7.00	N				7.2	4.0	17.9	40.0	0.0	0.0
CK W10	China	Kaili		Wuliu-Zengjiayan	10.00	N	14.0	72.0		0.0	0.0	0.0	0.0	0.0	0.0
CK W15	China	Kaili		Wuliu-Zengjiayan	15.00	N	38.0	15.0		9.2	3.5	0.0	32.4	0.0	0.0
CK W18	China	Kaili		Wuliu-Zengjiayan	18.00	N	40.0	29.0		3.7	5.5	8.9	0.0	12.0	0.0
CK W21	China	Kaili		Wuliu-Zengjiayan	21.00	N	19.0	40.0		0.0	6.3	18.6	0.0	16.1	0.0
CK W24	China	Kaili		Wuliu-Zengjiayan	24.00	N	51.0			6.7	0.0	0.0	42.3	0.0	0.0
CK W26	China	Kaili		Wuliu-Zengjiayan	26.00	N	30.0			20.7	4.2	0.0	45.2	0.0	0.0
CK W34	China	Kaili		Wuliu-Zengjiayan	34.00	N	35.0			5.4	0.0	0.0	60.6	0.0	0.0
CK W40	China	Kaili		Wuliu-Zengjiayan	40.00	N	41.0			12.9	4.8	0.0	40.3	0.0	0.0
CK W43	China	Kaili		Wuliu-Zengjiayan	43.00	N	35.0			9.9	0.0	0.0	55.1	0.0	0.0
CK W46	China	Kaili		Wuliu-Zengjiayan	46.00	N	30.0			18.5	6.6	0.0	45.9	0.0	0.0
CK W50	China	Kaili		Wuliu-Zengjiayan	50.00	N	41.0			11.5	5.0	0.0	41.5	0.0	0.0
CK W56	China	Kaili		Wuliu-Zengjiayan	56.00	N	24.0			19.4	3.4	0.0	53.2	0.0	0.0
CK W60	China	Kaili		Wuliu-Zengjiayan	60.00	N	32.0	25.0		0.0	19.2	0.0	23.8	0.0	0.0
CK W64	China	Kaili		Wuliu-Zengjiayan	64.00	N	12.0			8.5	0.0	0.0	65.5	0.0	0.0

Sample Name	Country	Stratigraphy				Contains BST fossils	Composition (% rock)								
		Formation	Member	Sequence	Height		Qtz	Calc	Dol	Bth	Gl	Cel	Il 1	Il 2	Kaol
CK M61	China	Kaili		Miaobanpo	61.00	N	10.0			4.6	4.1	0.0	42.3	0.0	0.0
CK M65	China	Kaili		Miaobanpo	65.00	N	6.0			13.7	9.7	0.0	68.6	0.0	0.0
CK M69	China	Kaili		Miaobanpo	69.00	N	31.0			0.0	3.4	0.0	54.6	0.0	0.0
CK M71	China	Kaili		Miaobanpo	71.00	N	34.0			5.5	6.9	0.0	54.5	0.0	0.0
CK M73	China	Kaili		Miaobanpo	73.00	N	33.0			6.4	0.0	0.0	59.6	0.0	0.0
CK M76	China	Kaili		Miaobanpo	76.00	N	38.0			5.9	2.9	0.0	31.2	0.0	0.0
CK M80	China	Kaili		Miaobanpo	80.00	N	34.0			4.1	0.0	0.0	61.9	0.0	0.0
CK M83	China	Kaili		Miaobanpo	83.00	N				18.0	0.0	0.0	82.0	0.0	0.0
CK M88	China	Kaili		Miaobanpo	88.00	N	29.0			5.7	0.0	0.0	53.3	0.0	0.0
CK M90	China	Kaili		Miaobanpo	90.00	N	39.0			2.8	0.0	0.0	43.2	0.0	0.0
CK M93	China	Kaili		Miaobanpo	93.00	N	34.0			4.2	0.0	0.0	49.8	0.0	0.0
CK M96	China	Kaili		Miaobanpo	96.00	N	46.0			4.2	0.0	0.0	48.8	0.0	0.0
CK M101	China	Kaili		Miaobanpo	101.00	Y	48.0			0.0	0.0	0.0	34.0	0.0	0.0
CK M102	China	Kaili		Miaobanpo	102.00	Y	43.0			6.6	0.0	0.0	44.4	0.0	0.0
CK M104	China	Kaili		Miaobanpo	104.00	Y	38.0			11.6	0.0	0.0	50.4	0.0	0.0
CK M116	China	Kaili		Miaobanpo	116.00	Y	51.0			0.0	0.0	0.0	32.0	0.0	0.0
CK M119	China	Kaili		Miaobanpo	119.00	Y	34.0			2.7	0.0	0.0	25.3	0.0	0.0
CK M121	China	Kaili		Miaobanpo	121.00	Y	51.0			1.6	0.0	0.0	35.4	0.0	0.0
CK M126	China	Kaili		Miaobanpo	126.00	Y	36.0			3.5	0.0	0.0	43.5	0.0	0.0
CK M129	China	Kaili		Miaobanpo	129.00	N	38.0			7.1	0.0	0.0	47.9	0.0	0.0
CK M131	China	Kaili		Miaobanpo	131.00	N	34.0			0.0	0.0	39.4	0.0	25.6	0.0
CK M134	China	Kaili		Miaobanpo	134.00	N				0.0	0.0	0.0	66.0	0.0	0.0
CK M136	China	Kaili		Miaobanpo	136.00	N	39.0			0.0	0.0	29.8	0.0	31.2	0.0
CK M138	China	Kaili		Miaobanpo	138.00	N	49.0			2.2	0.0	0.0	48.8	0.0	0.0
CK M141	China	Kaili		Miaobanpo	141.00	N	34.0			0.0	0.0	0.0	57.0	0.0	0.0
CK M144	China	Kaili		Miaobanpo	144.00	N	54.0			0.0	0.0	25.6	0.0	18.4	0.0
CK M147	China	Kaili		Miaobanpo	147.00	N	40.0			0.0	0.0	27.6	0.0	32.4	0.0
CK M149	China	Kaili		Miaobanpo	149.00	N	34.0			8.0	0.0	0.0	59.0	0.0	0.0

Sample Name	Country	Stratigraphy				Contains BST fossils	Composition (% rock)								
		Formation	Member	Sequence	Height		Qtz	Calc	Dol	Bth	Gl	Cel	Il 1	Il 2	Kaol
YPM 10470	China	Shipai				N				15.5	7.9	15.5	59.1	0.0	0.0
YPM 72897	Czechoslovakia	Etage C				N	58.0			0.1	2.0	0.0	32.0	0.0	0.0
YPM 154397	UK					N	34.0			18.0	17.5	0.0	0.0	26.5	0.0
YPM 163786	USA	Pioche	Pioche D			N				0.0	0.0	16.7	0.0	83.3	0.0
YPM 203937	USA	Campito	Montenegro			N	29.0			8.0	0.0	59.0	0.0	0.0	4.0
YPM 204003	USA	Latham				N	45.0			0.0	0.0	0.0	31.7	23.3	0.0
YPM 421785	China	Balang				N	59.0			0.0	0.0	25.5	16.5	0.0	0.0
YPM 424052	USA	Rogersville				N				11.5	0.0	0.0	88.5	0.0	0.0
YPM 424072	China	Balang				N	41.0	3.0		5.9	0.0	0.0	32.1	0.0	0.0
YPM 534372	USA					N		100.0		0.0	0.0	0.0	0.0	0.0	0.0
YPM 534374	USA	Meagher				N	18.0	56.0		0.0	12.6	11.4	0.0	0.0	0.0
OUMNH A.806	UK					N				0.0	9.5	6.2	60.3	0.0	0.0
OUMNH A.1752b- A.1753a	UK					N	30.0			17.1	8.9	1.5	0.0	19.5	0.0
OUMNH A.2325a	UK					N	55.0	14.0		1.5	4.9	1.2	0.0	2.4	0.0
OUMNH A.2346a	UK					N	37.0	4.0		17.2	13.5	0.0	1.9	13.4	0.0
OUMNH A.2361	UK					N	37.0			15.3	6.6	9.8	0.0	20.3	0.0
OUMNH A.2374	UK					N	42.0			16.1	16.7	2.7	0.0	22.5	0.0
OUMNH A.2470a	UK					N	38.0			12.8	11.1	0.0	6.3	18.8	0.0
OUMNH AT.93a	Canada	Hanford Brook				N	54.0			0.0	17.9	0.0	4.5	18.6	0.0
OUMN AT.103b	Canada	Hanford Brook				N	26.0			0.0	0.0	35.6	0.0	35.4	0.0
OUMNH AX.13	Morocco					N	16.0	23.0		0.0	12.8	23.2	0.0	0.0	0.0
OUMNH AX. 19a	Morocco					N	36.0			6.4	0.0	43.6	0.0	0.0	0.0
S7C_25	Canada	Stephen				Y	34.0	9.0		20.2	9.2	5.6	0.0	9.3	7.7
S7A_0_5	Canada	Stephen				Y	17.0	13.0		22.8	8.3	12.8	0.0	12.1	0.0
S7A_4	Canada	Stephen				Y	46.0			17.4	7.7	3.3	0.0	25.6	0.0
S7A_12	Canada	Stephen				Y	27.0	8.0		19.5	7.1	4.6	0.0	33.9	0.0
S7A_8	Canada	Stephen				Y	23.0	8.0		27.2	12.0	0.0	0.0	20.8	0.0

Sample Name	Country	Stratigraphy				Contains BST fossils	Composition (% rock)								
		Formation	Member	Sequence	Height		Qtz	Calc	Dol	Bth	Gl	Cel	Il 1	Il 2	Kaol
S7A_16	Canada	Stephen				Y	33.0	3.0		22.2	8.2	0.0	0.0	28.7	0.0
S7C_4_5	Canada	Stephen				Y	33.0	36.0	12.0	4.4	4.5	5.4	0.0	4.7	0.0
S7C_6	Canada	Stephen				Y	7.0	81.0		0.1	0.3	0.5	0.0	0.0	0.0
S7C_8	Canada	Stephen				Y			54.0	0.0	0.0	0.0	0.0	0.0	0.0
S7C_10_5	Canada	Stephen				Y			36.0	2.5	15.8	15.8	0.0	0.9	0.0
S7C_12	Canada	Stephen				Y		79.0	3.0	0.0	0.0	0.0	0.0	0.0	0.0
S7C_14	Canada	Stephen				Y	30.0	24.0		18.3	5.7	6.7	0.0	11.5	1.7
S7C_14_5	Canada	Stephen				Y	31.0	24.0		16.0	4.3	7.1	0.0	8.9	1.6
S7_15	Canada	Stephen				Y	24.0	20.0		18.5	5.1	6.1	0.0	11.3	0.0
S7_17	Canada	Stephen				Y	32.0	21.0		19.0	6.8	4.0	0.0	15.4	1.8
S7_19	Canada	Stephen				Y	34.0	5.0		19.5	5.3	0.0	0.0	13.0	5.3
S7_20	Canada	Stephen				Y	56.0			16.2	4.9	0.0	0.0	19.6	2.3
S7_22	Canada	Stephen				Y	18.0	2.0	7.0	19.6	6.8	0.0	0.0	35.7	4.8
S7_27_5	Canada	Stephen				Y	41.0	12.0		19.6	8.0	0.0	0.0	11.8	5.6
CL_1	USA	Latham Shale				N	27.0			16.2	0.0	0.0	0.0	47.8	0.0
CL_2	USA	Latham Shale				N	50.0			0.0	0.0	9.3	0.0	31.7	0.0
CL_3	USA	Latham Shale				N	40.0			0.0	0.0	7.1	0.0	43.9	0.0
CL_4	USA	Latham Shale				N	34.0			0.0	0.0	10.5	0.0	38.5	0.0
CL_5	USA	Latham Shale				N	33.0			0.0	0.0	6.4	0.0	60.6	0.0
CL_6	USA	Latham Shale				N	21.0			0.0	0.0	11.8	0.0	57.2	0.0
CPH_1	USA	Carrara				N				20.9	0.0	32.5	0.0	46.6	0.0
CPH_2	USA	Carrara				N	36.0	7.0		12.8	3.7	16.4	0.0	25.0	0.0
CPH_3	USA	Carrara				N	18.0			21.7	0.0	19.5	0.0	37.8	0.0
CPH_4	USA	Carrara				N				28.8	0.0	29.5	0.0	41.7	0.0
CPH_5	USA	Carrara				N	27.0			15.7	3.4	18.2	0.0	30.7	0.0
FP_1	Canada	Stephen	Burgess			Y		7.0	6.0	26.0	1.6	18.5	0.0	30.9	0.0

Sample Name	Country	Stratigraphy				Contains BST fossils	Composition (% rock)								
		Formation	Member	Sequence	Height		Qtz	Calc	Dol	Bth	Gl	Cel	Il 1	Il 2	Kaol
FP_2	Canada	Stephen	Burgess			Y	16.0	10.0		21.0	3.2	20.3	0.0	20.5	0.0
FP_3_7	Canada	Stephen	Burgess			Y	30.0	12.0		28.0	3.0	10.7	0.0	16.3	0.0
FP_4_9	Canada	Stephen	Burgess			Y	27.0	15.0	2.0	17.4	3.6	10.0	0.0	14.0	0.0
FP_6	Canada	Stephen	Burgess			Y	20.0	16.0		13.8	4.8	11.1	0.0	13.3	0.0
FP_7	Canada	Stephen	Burgess			Y	18.0	15.0		23.4	8.0	11.4	0.0	16.1	0.0
FP 8_9	Canada	Stephen	Burgess			Y		4.0	25.0	1.4	0.7	9.3	0.0	31.6	0.0
FP_9	Canada	Stephen	Burgess			Y	26.0	24.0		8.5	4.7	8.8	0.0	8.0	0.0
FP_10	Canada	Stephen	Burgess			Y	12.0	69.0	6.0	0.2	0.9	2.0	0.0	0.0	0.0
FP_11	Canada	Stephen	Burgess			Y	15.0	63.0	2.0	0.0	0.0	0.0	0.0	0.0	0.0
FP_12	Canada	Stephen	Burgess			Y	19.0	21.0	5.0	15.4	7.8	11.4	0.0	11.4	0.0
FP_20	Canada	Stephen	Burgess			Y	17.0	8.0	15.0	17.5	5.3	6.7	0.0	24.5	0.0
FP_20_5	Canada	Stephen	Burgess			Y	27.0	3.0		25.7	0.0	5.5	0.0	26.8	0.0
FP_21_8	Canada	Stephen	Burgess			Y	36.0			19.4	9.3	11.7	0.0	12.6	0.0
FP_22	Canada	Stephen	Burgess			Y	15.0	25.0		15.4	14.6	14.3	0.0	9.7	0.0
FP_23	Canada	Stephen	Burgess			Y	17.0	11.0	14.0	11.0	5.6	12.0	0.0	22.4	0.0
FP_24	Canada	Stephen	Burgess			Y	27.0	31.0		7.8	7.3	7.6	0.0	3.3	0.0
FP_25	Canada	Stephen	Burgess			Y	21.0	28.0		11.1	8.0	9.0	0.0	6.9	0.0
FP_26	Canada	Stephen	Burgess			Y	30.0	6.0		23.3	4.2	5.4	0.0	13.1	0.0
FP_27	Canada	Stephen	Burgess			Y	28.0	16.0		12.6	4.5	11.6	0.0	7.2	0.0
FP_28	Canada	Stephen	Burgess			Y	39.0	6.0		17.0	3.3	4.8	0.0	19.0	0.0
FP_30	Canada	Stephen	Burgess			Y		9.0	1.0	26.2	12.2	9.5	0.0	29.0	0.0
FP_31	Canada	Stephen	Burgess			Y	22.0	26.0		11.3	6.5	7.6	0.0	9.7	0.0
FP_32	Canada	Stephen	Burgess			Y		9.0	2.0	16.8	21.7	2.5	0.0	32.0	0.0
FP_33	Canada	Stephen	Burgess			Y	4.0	2.0		14.0	0.0	24.7	0.0	47.3	0.0
FP_35	Canada	Stephen	Burgess			Y	18.0	5.0		20.9	11.6	4.0	0.0	27.5	0.0
FP_36	Canada	Stephen	Burgess			Y	28.0	2.0		21.3	10.5	0.0	0.0	31.1	0.0
FP_37	Canada	Stephen	Burgess			Y	37.0	3.0		11.2	9.8	0.0	0.0	24.0	0.0
FP_38	Canada	Stephen	Burgess			Y	19.0	8.0		21.9	7.3	3.9	0.0	27.9	0.0

Sample Name	Country	Stratigraphy				Contains BST fossils	Composition (% rock)								
		Formation	Member	Sequence	Height		Qtz	Calc	Dol	Bth	Gl	Cel	Il 1	Il 2	Kaol
FP_39	Canada	Stephen	Burgess			Y	27.0	14.0		16.0	8.8	9.9	0.0	24.4	0.0
OWC_0_12	USA	Pioche				N	37.0			15.6	9.0	0.0	0.0	30.4	0.0
OWC_0_28	USA	Pioche				N	26.0			16.5	7.5	12.5	0.0	28.5	0.0
OWC_0_32	USA	Pioche				N	24.0			17.6	9.8	12.9	0.0	28.7	0.0
OWC_0_38	USA	Pioche				N	22.0			20.9	11.1	5.8	0.0	40.2	0.0
OWC_1	USA	Pioche				Y	24.0			0.0	0.0	15.7	0.0	59.3	0.0
RW_1	USA	Pioche				N	30.0			17.2	0.0	28.0	0.0	24.9	0.0
RW_2	USA	Pioche				N	24.0			20.6	0.0	14.7	0.0	34.7	0.0
RW_3	USA	Pioche				N	44.0			9.9	0.0	18.8	0.0	21.3	0.0
RW_4	USA	Pioche				N	40.0	3.0		13.0	1.6	16.5	0.0	26.0	0.0
RW_5	USA	Pioche				N	27.0			15.3	0.0	16.9	0.0	40.8	0.0
RW_6	USA	Pioche				N				23.4	3.1	24.9	0.0	48.5	0.0
WHY_S_41	Canada	Stephen	Burgess			Y	68.0		6.0	0.0	0.0	0.0	0.0	0.0	0.0
WHY_S_43	Canada	Stephen	Burgess			Y		42.0	31.0	0.0	0.0	0.0	0.0	0.0	0.0
WHY_S_47	Canada	Stephen	Burgess			Y	18.0	4.0		32.9	5.5	9.2	0.0	20.4	0.0
WHY_S_51	Canada	Stephen	Burgess			Y	24.0	7.0		27.5	3.2	8.5	0.0	20.8	0.0
WHY_S_53	Canada	Stephen	Burgess			Y	34.0	36.0		7.0	7.4	7.1	0.0	4.4	0.0
WHY_S_55	Canada	Stephen	Burgess			Y	17.0	19.0	3.0	19.2	8.4	10.8	0.0	11.6	0.0
WHY_S_45_(5)	Canada	Stephen	Burgess			Y		53.0	12.0	0.0	0.0	0.0	0.0	0.0	0.0
YPM 200359	USA	Wheeler				Y	28.0	40.0		8.4	6.7	7.6	7.3	0.0	0.0
YPM 219298	Canada	Stephen				Y	33.0	5.0	2.0	13.0	16.3	0.0	0.0	19.7	0.0
YPM 424000	China	Kaili				Y	47.0			9.2	3.4	0.0	40.3	0.0	0.0
YPM 529546	USA	Langston	Spence			Y		6.0		26.6	10.9	2.9	0.0	47.7	0.0
YPM 533117	USA	Wheeler				Y	25.0	20.0		13.1	5.9	15.4	0.0	10.6	0.0
YPM 534367	Canada	Stephen	Burgess			Y	33.0	9.0		12.1	17.0	0.0	0.0	26.9	0.0
YPM 14392	USA	Kinzers				Y	18.0			11.7	0.0	62.8	0.0	2.7	4.8

Table S1: Sample identifications and mineralogical composition. Abbreviations: Qtz = quartz, Calc = calcite, Dol = dolomite, Bth = berthierine/chamosite, Gl = glauconite, Cel = celadonite, Il 1 = illite composition 1, Il 2 = illite composition 2, Kaol = kaolinite.